Design of a Wideband, High Steering Angle and Low Side-Lobes Levels Matrix Antenna

Paul Karmann[1,*], Edson Martinod[2], Eric Arnaud[3], Joël Andrieu[4]
[1]DGA Maîtrise de l'Information – BP 7 - 35998 Rennes Cedex 9, France,
Email: paul.karmann@unilim.fr
[2]XLIM, University of Limoges, RF Systems, 7 rue Jules Vallès, 19100 Brive-la-Gaillarde, France,
Email: edson.martinod@xlim.fr
[3]XLIM, University of Limoges, RF Systems, 123 Av. Albert Thomas, 87000 Limoges, France,
Email: eric.arnaud@xlim.fr
[4]XLIM, University of Limoges, RF Systems, 7 rue Jules Vallès, 19100 Brive-la-Gaillarde, France,
Email: joel.andrieu@xlim.fr
[*] *Corresponding author*

Abstract: **This paper presents the use of pixel-type radiating elements in the context of broadband beam steering. The elements are composed of a resonant cavity topped by a frequency selective surface, fed via a patch antenna and filled with dielectric substrates. This pixel antenna has a wide -10 dB matching band from 1.22 to 1.61 GHz, which corresponds to a 27% fractional bandwidth. It has an angular aperture greater than 124° and a realized gain between 3.3 and 3.8 dBi over the whole matching band. An array composed of 5 elements has been simulated and allows a steering on a range of ±60° in the E plane while keeping the gain variation below 3 dB. A prototype has been manufactured and presents a steering capacity between -56 and 53° on the whole band with side-lobes levels lower than -8.1 dB whatever the angle.**

Keywords: **Periodic structures, Metasurface, Beam steering, Wideband antenna.**

I. INTRODUCTION

Whether for defence or telecommunications applications, the need for broadband antennas capable of achieving high angular steering, for up to ±60° and higher, is increasing. These antennas must achieve those performances while maintaining relatively low side-lobes levels (SLLs).

In order to remove the array lobes that appear during steering, the individual elements of the antenna array must comply with (1) [1]:

$$d_{max} = \frac{\lambda}{1 + \sin(\theta)} \quad (1)$$

This formula defines the maximum distance d_{max} at which the grating lobes start to appear as a function of λ the working wavelength and θ the steering angle. The antennas must also have a large half-power beam-width (HPBW) to allow a good gain to be maintained during steering. Among the technologies that allow to achieve high steering angle are reconfigurable structures, which use active devices to modify the characteristics of the antenna during operation. This allows for example to change the radiation pattern of the antenna, thus limiting the need for a large HPBW and increasing the gain. These reconfigurations can be realized by using P-i-N diodes [2] or varactors [3], which effectively change the shape of the antenna. The use of multiple feed ports [4] or phase shifters [5,6] is also a possibility to achieve such reconfigurations. The main issue with the use of patch antennas is their low bandwidth. In order to improve it, it is possible to use non-rectangular patches [7], cavity-backed structures [8-11] or stacked-patches [12].

The use of cavities also makes it possible to meet the need for large HPBW, via the use of metamaterial type structures [13,14]. Other techniques consist in the use of protrusions [15] or metallic walls [16], which induce a different distribution of the field emitted by the patch.

Among those potential technologies, the agile radiating matrix antennas (ARMA) have proven to be able to achieve wide beam steering with low side-lobes levels and high fractional bandwidth around 25% [17]. Those antennas are composed of a resonant cavity excited by a patch antenna, which allows it to achieve a wide bandwidth [18] and topped by a frequency selective surface (FSS). It creates a resonant cavity while placed in the broadside direction [18-20] and allows for a reduction of the height of the cavity [21]. The antennas, which are commonly called pixels, are able to be used alone thanks to their wide half-power beam-width (HPBW) [22] or are placed without any air gap in an array [20]. In this configuration, the array is able to achieve high steering angle with low side lobes levels, which is of interest for a steering application [23].

However, the antenna is not able to achieve a high steering angle over all of its bandwidth. This is due to the large width of the pixel in regard of the wavelength. Indeed, the pixels are classically designed to achieve high gain and as such are 0.5*λ wide at the lowest working frequency [18]. It is however possible to achieve a lower size by adding a dielectric substrate inside the antenna cavity [24]. This reduces the bandwidth of the antenna but eliminate possible SLLs over the whole bandwidth. In light of those good performances, an antenna has been designed to achieve a good steering with optimal coverage of global navigation satellite system (GNSS) frequencies in L band. The steering

capacity required for this antenna is about 60° in both directions in the E plane.

The first part of this paper presents the design considerations of the pixel antenna and its dimensions. The array and its steering capacities are then investigated in simulation. The second part presents the manufactured array and the tests results. Finally, a conclusion presents a summary and concluding remarks.

II. SIMULATED ANTENNA DIMENSIONS AND DESIGN CONSIDERATIONS

As the antenna is intended to operate at frequencies starting at f_0 = 1.2 GHz without SLLs, its size must be reduced compared to the standard design, which is 0.5 * λ_0 in width, with λ_0 the wavelength at the low frequency. The reduction method presented in [24] has been used to improve the steering performances of the array. The designed pixel has a width of 76 mm, which corresponds to 0.31 * λ_0. Since the purpose of the study is to make a prototype, the materials are chosen with regard to their cost. Thus, some materials may have high electrical losses. This is the case of the FR-4 on which the FSS has been printed, which possess a permittivity of 4.6 and a tan(δ) = 2.5 * 10^{-2}. The patch antenna is placed on a PEEK substrate with ε_r = 3 and tan(δ) = 2.7 * 10^{-3} and the cavity is filled with an HDPE substrate with ε_r = 2.25 and tan(δ) = 2 * 10^{-4}. The components and the geometrical dimensions of the pixel are presented in Fig. 1 and the dimensions are compiled in Table 1.

TABLE I: GEOMETRICAL DIMENSIONS OF THE SIMULATED PIXEL

Parameter	Dimension (mm)	Parameter	Dimension (mm)
L_s	76	h	26.6
L	57.7	W	19.2
H_{PEEK}	8.4	H_{HDPE}	17.2
H_{FR-4}	1	L_c	16.8
L_{FSS}	22.1	d_{FSS}	3.3
R_{FSS}	2.9	R_{cavity}	15
R_{Patch}	1.5		

The antenna is simulated with CST Microwave Studio with two configurations. Indeed, in order to characterize the antenna experimentally, it is necessary to add a support device. Due to the configuration of the measuring facility, it is not possible to use a smaller support structure. Fig. 2.a shows the configuration using this device. The pixel without such device is also simulated to provide a basis for comparison. It is notable that the dimension of the fixing system is substantial in relation to the lateral dimension of a single pixel. This can lead to many alterations of the radiation and the functioning of the pixel, which must be taken into account in the simulation. In order to reduce the influence of this element as much as possible, the fixation spacers were made of a PEEK material with the same characteristics as the one used in the pixel design.

The gains and adaptations of these two configurations are presented in Fig. 2.b for the pixel-only configuration and Fig. 2c for the configuration with fixation. The pixel taken alone has a -10 dB adaptation band from 1.21 to 1.61 GHz which corresponds to a 28% fractional bandwidth. Its directivity is relatively stable over its adaptation band with a value close to 5 dBi. The high dielectric losses of the materials and the adaptation close to -10 dB at 1.4 GHz cause a decrease of the realized gain to a value of 4.3 dBi at this frequency. Its value is 4.6 dBi at the frequency of 1.2 GHz. Using the support structure, the matching band at -10 dB is 1.22 to 1.61 GHz, which corresponds to a fractional band of 27%. Between 1.37 and 1.45 GHz, the interactions with the support cause the adaptation to go above -10 dB, with a maximum of -9.5 dB. The directivity of the pixel is also affected by the presence of the structure. Indeed, it decreases with frequency and reaches 3.8 dBi at 1.55 GHz. This decrease is maintained for the realized gain, which has a value between 3.3 dBi and 4.3 dBi on the adaptation band with a minimum at 1.45 GHz. In both cases, it can be noticed that there is jumps in directivity around 1.8 GHz. This is related to a strong variation of the HPBW around

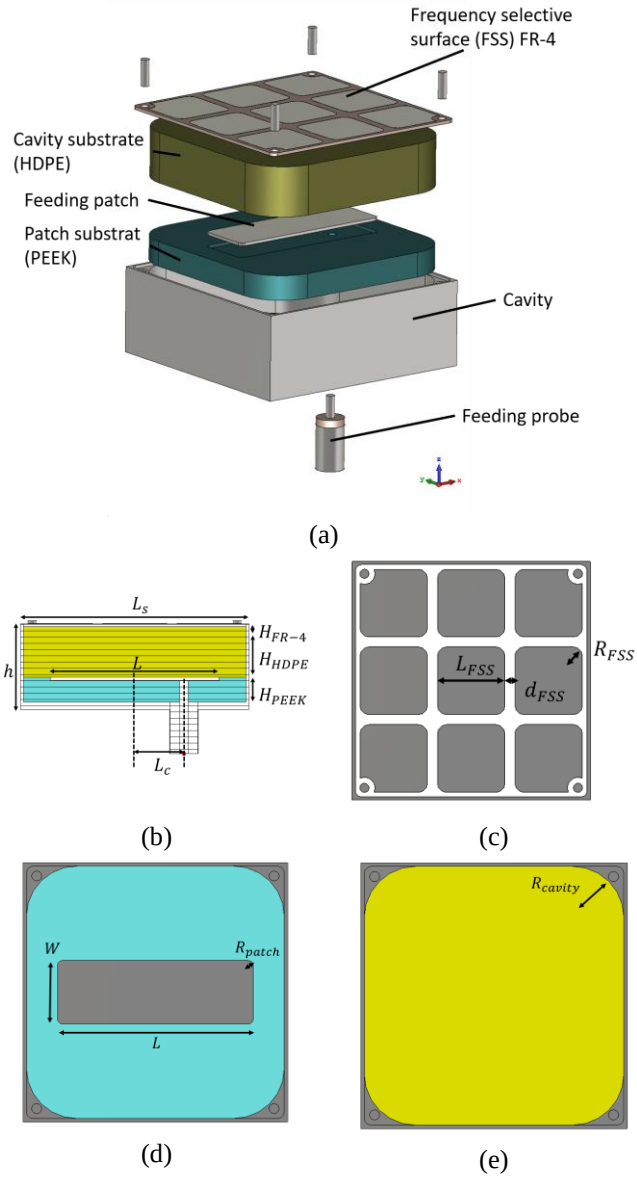

Fig. 1. Geometrical dimensions of the simulated pixel: (a) Exploded view of the pixel (b) Cut view of the element. (c) View of the FSS. (d) View of the excitation patch. (e) View of the cavity.

these frequencies. Furthermore, the directivity is given here in the broadside direction of the antenna and therefore only takes into account the variations in this direction.

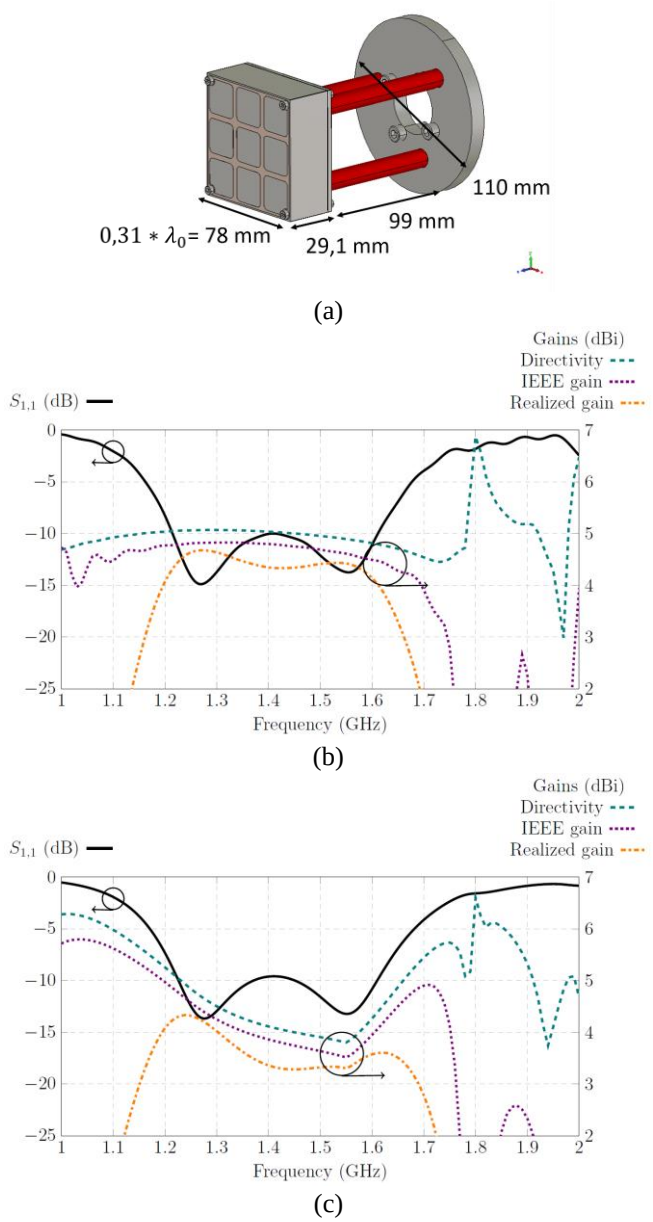

Fig. 2. Pixel with the support device and simulation characteristics: (a) Simulated pixel with support structure. (b) Parameters of the pixel without the support structure. (c) Parameters of the pixel with the support structure.

The radiation patterns at high-low and centre frequencies have been plotted in Fig. 3 for both configurations. Markers indicating the angles corresponding to the gain values at -3 dB from maximum were also added. In both configurations, the HPBW of the antenna is greater than 119° regardless of the frequency. The plots show a slight in-plane asymmetry, which is especially visible at high frequencies. This is due to the position of the feeding patch in the pixel cavity. Since the HPBW increases with frequency, this does not pose major problems for radiation and future beam steering and is the reason of the low augmentation of the gain in the higher frequencies. This large HPBW is also the source of the variations that are observed when using the fixation system. A possible way to reduce its impact is to add absorbing foams during the measurement. The diagrams are indeed strongly modified when using it, with changes in gain which correspond to the values observed in Fig. 2.c. The HPBW is increased by the presence of the fixation device, with a value higher than 124° and the asymmetry is also present in the antenna.

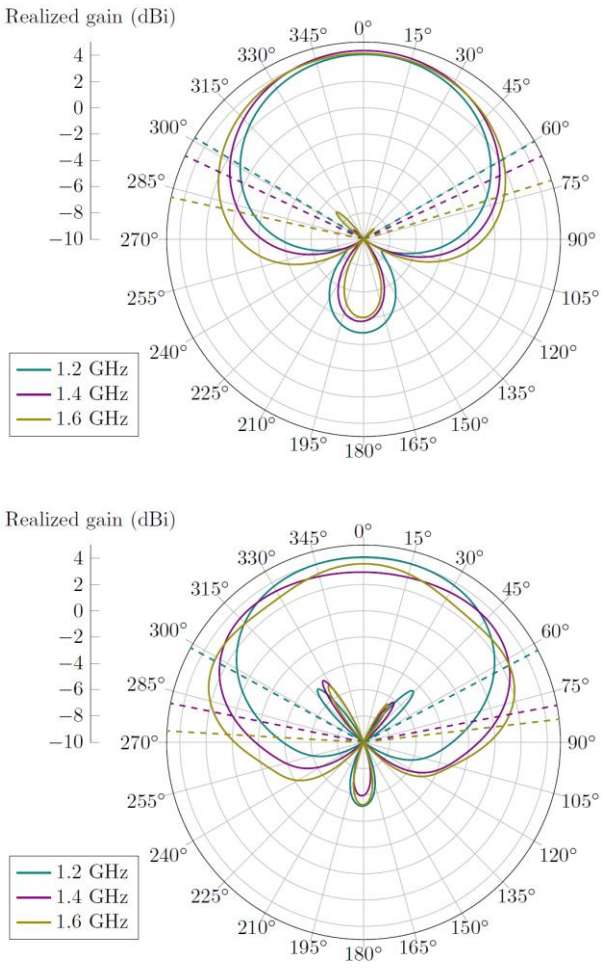

Fig. 3. Realized gain patterns in the E-plane of the pixel antenna for 1.2, 1.4 and 1.6 GHz: (a) Without the metallic mount. (b) With the metallic mount.

III. SIMULATED ARRAY AND STEERING CAPACITY

In order to show the beam steering capabilities of the antenna, an array composed of five elements was simulated. This number of elements was selected to consider the fabrication of a prototype. The simulated array uses the same support system presented previously.

The steering of the array is produced by changing the phases at the entrance of each pixel. The magnitude is uniform over the whole array. The phases come from (2) [1] and are multiplied by the position of the pixel. As such, the first pixel has a phase of 1*φ and the fifth of 5*φ. The angle θ corresponds to the steering angle set for the array, and λ to the wavelength at the current frequency. d corresponds classically to the distance between two phase centers. With the ARMA technology, this corresponds to the width of the elements [21].

TABLE II: STEERING ANGLES OBTAINED FOR A θ SETPOINT WITH REALIZED GAINS AND CORRESPONDING SLLS FOR THE SIMULATED ARRAY.

θ (°)	1.2 GHz Achieved Angle (°)	1.2 GHz Realized Gain (dBi)	1.2 GHz SLLs (dB)	1.4 GHz Achieved Angle (°)	1.4 GHz Realized Gain (dBi)	1.4 GHz SLLs (dB)	1.6 GHz Achieved Angle (°)	1.6 GHz Realized Gain (dBi)	1.6 GHz SLLs (dB)
-90	-60	8.6	-9.0	-61	9.1	-8.0	-63	9	-8.1
-60	-55	8.3	-10.4	-54	9.4	-9.5	-55	-9.5	-9.9
-30	-27	6.9	-10.3	-27	9	-10.7	-28	10.3	-10.8
0	-1	7	-10.9	-1	9.5	-11.7	-1	11	-12.3
30	27	6.8	-10.5	28	9	-10.8	28	10.3	-11.0
60	55	8.3	-10.4	55	9.4	-9.6	56	9.5	-10.1
90	61	8.6	-8.7	61	9	-8.0	63	8.9	-8.1

$$\varphi = \frac{360 * d * \sin(\theta)}{\lambda} \quad (2)$$

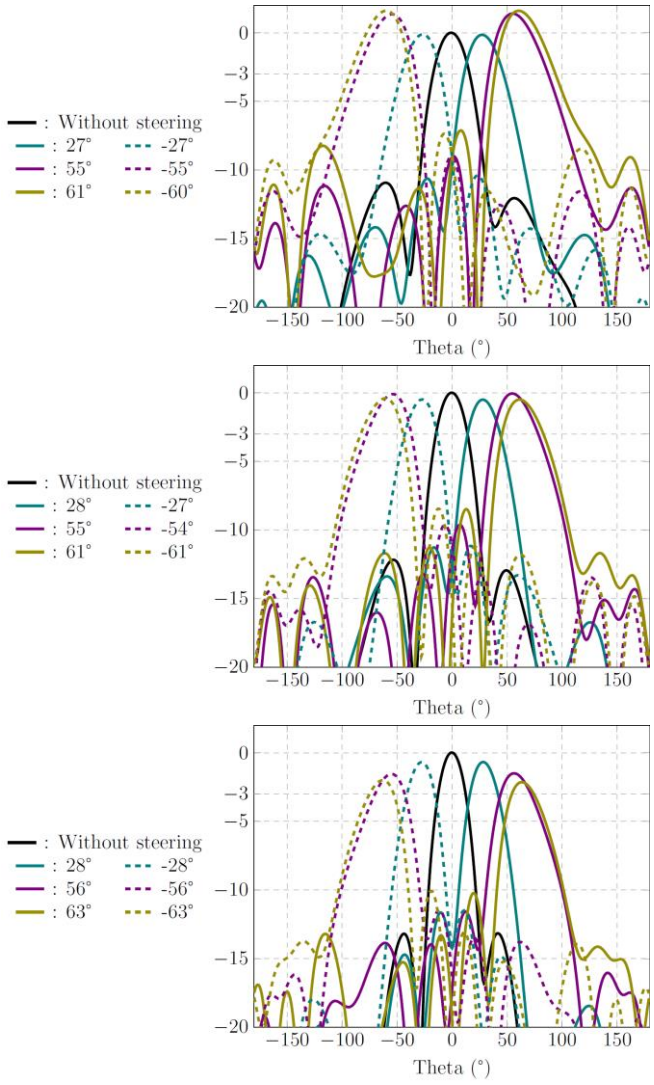

Fig. 4. Normalized realized gain for different steering angles of the simulated array in the E-plane: (a) At 1.2 GHz and normalized at 6.96 dBi. (b) At 1.4 GHz and normalized at 9.53 dBi. (c) At 1.6 GHz and normalized at 11 dBi.

The steering angles achieved by the array are shown in Fig. 4. To allow a good visualization of the gain variations and SLLs, their value has been normalized to the value without steering. It is noteworthy that the gain increases with the angle for the low frequencies. This is particularly noticeable for the 1.2 GHz frequency where the gain at maximum steering angle is 1.3 dB higher than the gain without steering. This is due to the effect of the back lobes which participate in the radiation of the array. They also have the effect of widening the main lobe. This phenomenon is shown in Fig. 5. The angles presented are between θ=-25° and θ=-45° in order to better visualize the evolution of the lobes. The angle reached by the main lobe increases while the back lobe, located around -125° remains stable. The lobes are thus approaching each other during the increase of the steering. The value of the back lobe decreases before being integrated into the main lobe, starting θ=-40°, which undergoes a widening of its width as well as an increase of its value.

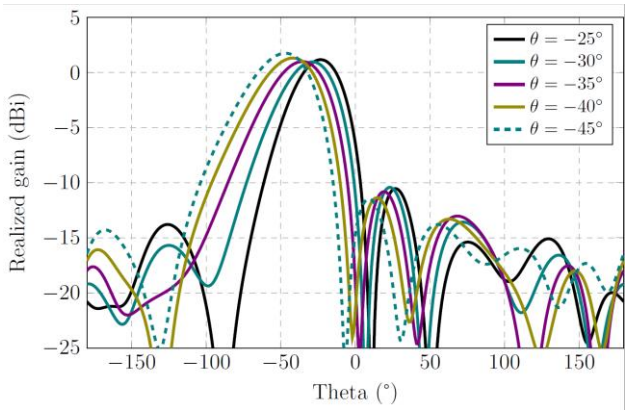

Fig. 5. Variation of the steering angle at 1.2 GHz on a 5-elements antenna to showcase the contribution of the back lobes.

For all frequencies and all offset angles, the array maintains a realized gain within a margin of less than 3 dB. Moreover, its gain for the maximum offset angles is very close, with a variation of less than 0.5 dB. This result is presented in Fig. 6. In order to obtain a simulation close to the future measurement, it takes into account the losses in the supply circuit that will be used during the experimental measurement.

TABLE III: STEERING ANGLES OBTAINED FOR A θ SETPOINT WITH REALIZED GAINS AND CORRESPONDING SLLS FOR THE MEASURED ARRAY.

θ (°)	1.2 GHz Achieved Angle (°)	1.2 GHz Realized Gain (dBi)	1.2 GHz SLLs (dB)	1.4 GHz Achieved Angle (°)	1.4 GHz Realized Gain (dBi)	1.4 GHz SLLs (dB)	1.6 GHz Achieved Angle (°)	1.6 GHz Realized Gain (dBi)	1.6 GHz SLLs (dB)
-90	-56	8.7	-9.3	-56	8.7	-8.3	-62	8.8	-8.1
-60	-51	8.4	-10.8	-51	9.4	-10.3	-56	9.6	-8.4
-30	-26	7	-10.3	-27	8.8	-10.4	-29	10.3	-10.3
0	-2	7.3	-10.5	-2	9.3	-10.5	-3	11.1	-11.3
30	25	7	-9.9	25	9.1	-9.8	27	10.2	-10.0
60	48	8.5	-10.0	49	9.4	-10.6	52	9.2	-9.1
90	53	8.8	-9.4	55	8.9	-9.1	59	8.6	-8.3

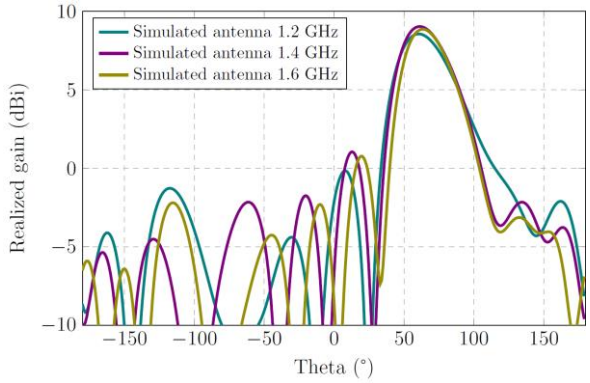

Fig. 6. Maximum steering angle of the simulated array for three frequencies.

The data presented in Fig. 4 and the side-lobes levels are compiled in Table II. It is noticeable that the results are relatively symmetrical for all frequencies but that a slight improvement of the steering towards the positive angles can be observed. This is, as is the case for the single pixel, due to the position of the feed in the cavity. However, the gains are slightly higher for the negative angles. Overall, the results of the array are found to be satisfactory as the antenna is able to achieve high steering with low SLLs levels on its whole band while using a low number of elements. This led to the realization of a prototype aimed at validating them.

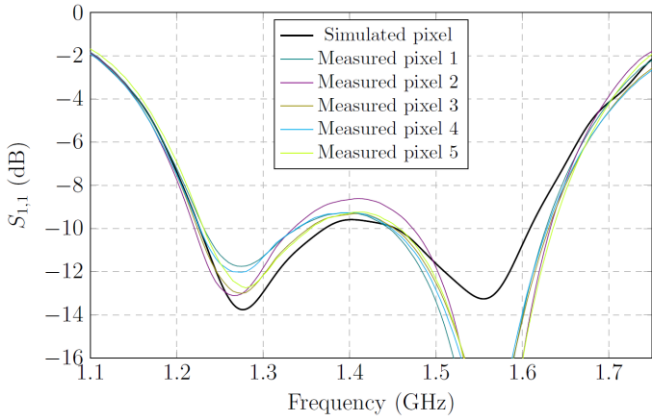

Fig. 7. Comparison between the simulated pixel with the metallic support device and the manufactured pixels measured alone in terms of reflection coefficient.

IV. MANUFACTURED PIXEL PERFORMANCES

In light of these good results, five elements have been manufactured. The pixels were measured separately to validate their radiation and adaptation characteristics and to compare these values to the simulations. Measurements were performed at the far-field antenna test range of the PLATINOM platform [25]. The measured adaptation is presented in Fig. 7 and shows a good similarity between the results. The simulated pixel used for the comparison here is the pixel using the fixation device in order to get closer to reality. In general, the manufactured pixels have a behaviour close to that expected in simulation. However, there is a notable difference at the higher frequencies. A retro-simulation has shown that this comes from a manufacturing deviation related to the fixation of the FSS to the metal cavity, the clamping screws deforming it slightly. It should be noted that the adaptation of pixel 2 is slightly deteriorated compared to other elements, this comes from a defect in the soldering of the connector to the feeding patch.

The measured gains are presented in Fig. 8 and show a good correlation with the simulation, but there is a difference in the high frequencies. This comes from the better adaptation of the pixels to these frequencies.

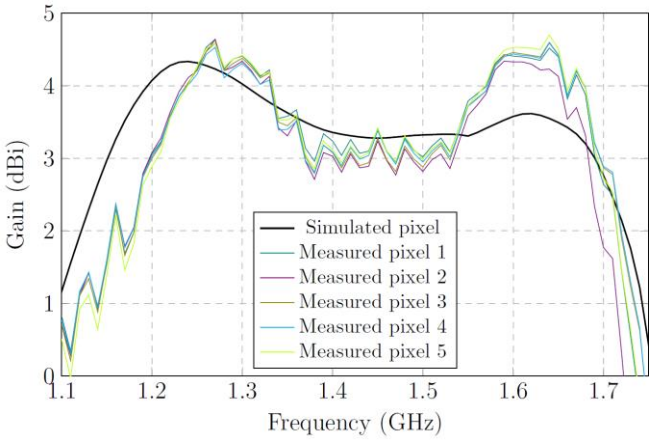

Fig. 8. Comparison between the simulated pixel with the metallic support device and the manufactured pixels measured alone in terms of realized gain.

V. STEERING CAPACITY OF THE MANUFACTURED ANTENNA

The pixels are positioned in an array presented with the measurement setup in Fig. 9. In order to allow the steering, phase shifters and delay lines have been used. The input phases of each feed correspond to the values calculated with (2) and allow to obtain the realized gains presented in Fig. 10. The latter have also been normalized in order to allow a better comparison with the simulated gains. The maximum steering angle is 53° for 1.2 GHz and 59° for 1.6 GHz.

Contrary to the simulation, the array achieves here a better angle in the negative beam steering. The gains show the same phenomenon of increase with the angle of steering observed during the simulation and their variations are also contained within a margin of 3 dB. The differences between the gains at the maximum offsets is 0.5 dBi for the negative angles and 0.8 dBi for the positive angles.

The deviations between the simulated and measured results can be attributed to the manufacturing process but remain within a suitable margin. It is also worth taking into account that the presence of the feeding circuit is also a source of notable differences and that the measurement environment is not ideal. This is linked to a tolerance of about 0.45 dB on the realized gain of the measurement platform.

(a)

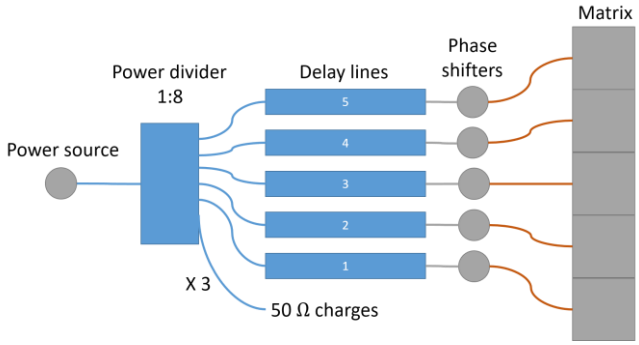

(b)

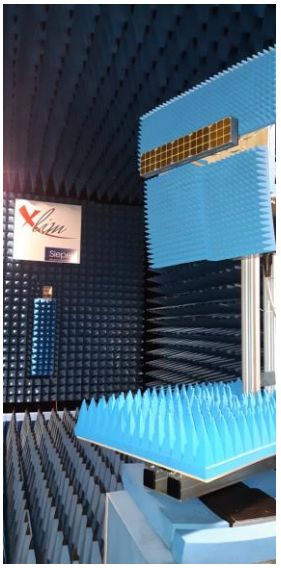

(c)

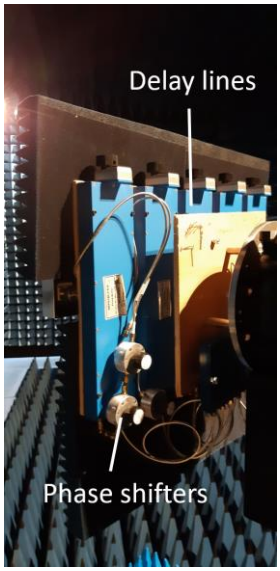

(d)

Fig. 9. View of the manufactured antenna: (a) View of the antenna. (b) Connection diagram of the array. (c) Measurement setup from the front. (d) Measurement setup from the back.

A comparison between the maximum steering angles of the simulated and fabricated is shown in Fig.11. It shows a good correlation between the values of the main lobe gains of the two matrices.

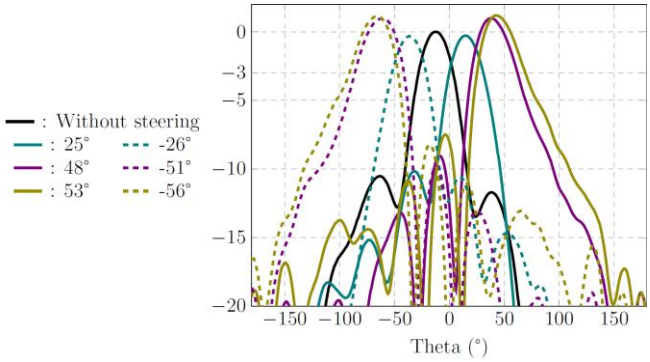

(a)

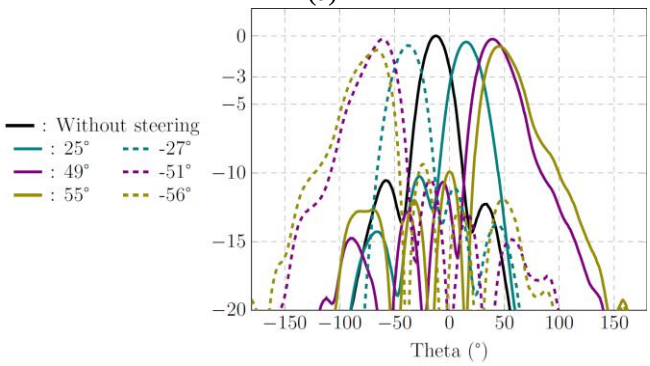

(b)

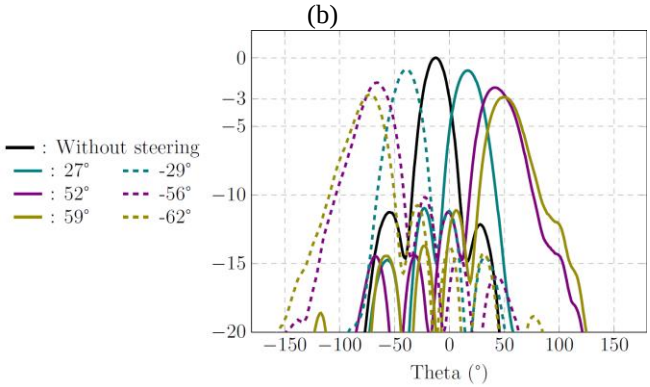

(c)

Fig. 10. Normalized realized gain for different steering angles of the realized array in the E-plane: (a) At 1.2 GHz and normalized at 7.3 dBi. (b) At 1.4 GHz and normalized at 9.3 dBi. (c) At 1.6 GHz and normalized at 11.1 dBi.

The SLLs are compared in Fig12. The simulated array shows a slight difference in both directions due to the position of the feed in each pixel. It is also noticeable that the SLLs increase sharply when the steering angle exceeds 55° in both directions. Below these values, the SLLs are less than -9.6 dB. For the manufactured array, it is notable that the values at 1.6 GHz increase faster with angle. The later also has higher SLLs at positive angles than the simulated array. Some of these differences may stem from the small number of measurement points that could be performed. The array has SLLs less than -8.1 dB for its entire frequency and steering range.

Table III presents a compilation of the results of the fabricated array. For set angles less than 60°, the array shows good symmetry both in achieved angle and in gain

and SLLs values. However, it is notable that a 3° deviation of the achieved angle is observed. This may be due to the manual phase shift used during the manipulations. Although an absorbing foam was used, the size of the delay lines can also be the source of deviations related to back reflections.

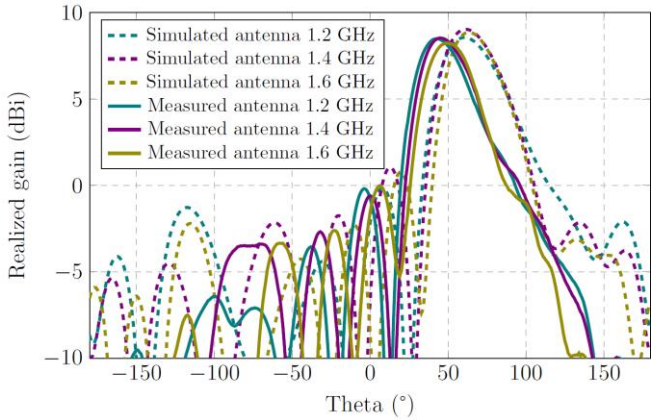

Fig. 11. Maximum steering angle of the measured array for three frequencies.

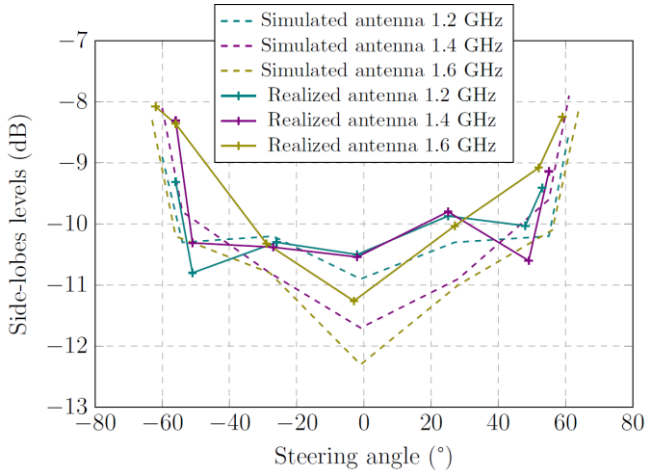

Fig. 12. Side-lobes levels of the measured array as a function of angle for different frequencies.

Table IV presents a comparison of the performances achieved by these works with others from the literature. It is notable that the technologies presented in [2,4,5] use reconfigurable technologies, which allows them to achieve high steering with a small number of elements and with low SLLs. However, these technologies lack wide bandwidth. The technologies presented in [9, 26-29] show a difficulty in reconciling bandwidth, high steering angles and low SLLs even when using the same technology. Compared to [20] and [24], which also uses MARPEM technology, the work presented here has a lower scan range and higher SLLs but has a higher bandwidth and a low number of elements. Overall, the work presented in this paper achieves a good balance between all parameters while keeping the number of elements low. This is particularly important considering the complexity, size and cost of a large beamforming network. A small number of elements is also required for certain types of applications where the network is mounted on a compact system. A higher steering can be obtained by increasing the number of elements composing the array, bringing it closer to an infinite array, this leads to a decrease in the width of the main lobe, an increase in the achieved steering angle and a reduction in the contribution of the back lobes.

TABLE IV: COMPARISON OF THE SCANNING PERFORMANCES BETWEEN THIS WORK AND [2,4,5,9,20,24,26-29].

Reference	Relative BW	Peak SLLs	Scan Range	Number of Elements
[2]	5%	-7.8 dB	150°	4
[4]	2%	-10.1 dB	144°	5
[5]	3.3%	-8.8 dB	162°	4
[9]	11.5%	-13 dB	120°	5
[26]	18%	-4.9 dB	144°	8
[27]	3%	-15 dB	140°	16
[28]	17%	-3 dB	180°	9
[29]	24%	-5 dB	171°	4
[20]	4%	-11 dB	140°	17
[24]	20%	-8 dB	140°	11
This Work	27%	-8.1 dB	109°	5

VI. CONCLUSION

In this paper, a pixel antenna has been designed with the objective of operating in the GNSS band with a large beam steering capability. This antenna consists of a metallic cavity fed by a patch antenna and filled with a dielectric. The cavity is topped by an FSS and allows to obtain a fractional matching band of 27%. An array composed of five elements has been simulated and realized, allowing to obtain a steering angle between -56 and 53° on the whole operating band and for all frequencies. Moreover, the SLLs are kept below -8.1 dB in all cases. Future work will focus on improving the steering capability of the structure and reducing the mutual coupling between the different elements. Initial work has already been carried out through the use of soft electrical surfaces [30].

ACKNOWLEDGMENT

This work was supported in part by the French Ministry of Defence via the Defence Innovation Agency (AID).

This work was supported in part by the society ITOPP.

PLATINOM facility is supported by the european regional development foundation and the New Aquitaine region (FEDER-PILIM 2015-2020 New Aquitaine).

REFERENCES

[1] S. Drabowitch, A. Papiernik, H. Griffiths, J. Encinas, and B. L. Smith, *Modern antennas*. Springer Science & Business Media, 2010.

[2] X. Ding, Y. Cheng, W. Shao, and B. Wang, "A wide-angle scanning phased array with microstrip patch mode reconfiguration technique," *IEEE Transactions on Antennas and Propagation*, vol. 65, no. 9, pp. 4548–4555, 2017.

[3] C. J. You et al., "Frequency- and Pattern-Reconfigurable Antenna Array with Broadband Tuning and Wide Scanning Angles," *IEEE Transactions on Antennas and Propagation*, vol. 71, no. 6, pp. 5398-5403, 2023, DOI: 10.1109/TAP.2023.3255647.

[4] Y. Cheng, X. Ding, W. Shao, M. Yu, and B. Wang, "2-d planar wide-angle scanning-phased array based on wide-beam elements," *IEEE Antennas and Wireless Propagation Letters*, vol. 16, pp. 876–879, 2017.

[5] Z. Chen, Z. Song, H. Liu, X. Liu, J. Yu, and X. Chen, "A compact phase-controlled pattern-reconfigurable dielectric resonator antenna for passive wide-angle beam scanning," *IEEE Transactions on Antennas and Propagation*, vol. 69, no. 5, pp. 2981–2986, 2021.

[6] K. Wang et al., "A Novel Low-Profile Phased Antenna with Dual-Port and Its Application in 1-D Linear Array to 2-D Scanning," *IEEE Transactions on Antennas and Propagation*, vol. 70, no. 8, pp. 6718-6731, 2022. DOI: 10.1109/TAP.2022.3161339

[7] A. A. Deshmukh, A. A. Desai, P. Kadam, and K. P. Ray, "Ultra-wide band e-shaped patch antenna," *2016 IEEE Annual India Conference (INDICON)*, pp. 1–5, 2016.

[8] W.-M. Zou, S.-W. Qu, and S. Yang, "Wideband wide-scanning phased array in triangular lattice with electromagnetic bandgap structures," *IEEE Antennas and Wireless Propagation Letters*, vol. 18, no. 3, pp. 422–426, 2019.

[9] L. Yi, H. Yu, Y. Yin, Y. Tian and Y. Yu, "Wideband SIW Cavity-backed Microstrip Antenna for Wide-angle Scanning Phased Array," *2021 CIE International Conference on Radar (Radar*), China, pp. 2681-2684, 2021. DOI: 10.1109/Radar53847.2021.10027867.

[10] F. -L. Jin, W. Shao, L. -Y. Xiao, B. -Z. Wang and B. Jiang, "Substrate-Integrated Cavity-Backed Array with Controlled Mutual Coupling for Wide Scanning," *IEEE Antennas and Wireless Propagation Letters*, vol. 21, no. 4, pp. 808-812, 2022. DOI: 10.1109/LAWP.2022.3149032.

[11] S. Ikeda, K. Yokokawa, N. Nakamoto, T. Fukasawa, M. Ohtsuka and Y. Inasawa, "A Circularly Polarized Cavity-Backed Stacked Patch Antenna for Wide-Angle Beam Scanning Millimeter-Wave Phased Array," *2020 International Symposium on Antennas and Propagation (ISAP)*, Osaka, Japan, pp. 721-722, 2021. DOI: 10.23919/ISAP47053.2021.9391252.

[12] C. Yang, S. Feng, and S. Liu, "Microstrip aperture-coupled stacked patch antenna array for wide-band wide-angle-scan applications," 2018 *Asia-Pacific Microwave Conference (APMC)*, pp. 594–596, 2018.

[13] L. Garcia-Gamez, L. Bernard, R. Sauleau, S. Collardey, K. Mahdjoubi, P. Pouliguen, and P. Potier, "Circularly-polarized GNSS metasurface antenna with two feed points in a sub-wavelength metallic cavity," *2022 16th European Conference on Antennas and Propagation (EuCAP)*, pp. 1–4, 2022.

[14] Z. Wang and Y. Dong, "Metamaterial-Based, Wide-Angle Beam-Scanning Array with Pattern Reconfigurable Element for 5G Base Station Applications," *2021 IEEE International Workshop on Electromagnetics: Applications and Student Innovation Competition (iWEM)*, Guangzhou, China, pp. 1-2, 2021. DOI: 10.1109/iWEM53379.2021.9790679.

[15] S. Ye, X. Liang, J. Geng, and R. Jin, "Wideband wide-slot antenna array with protrusion for wide-angle scanning," *2017 IEEE International Symposium on Antennas and Propagation USNC/URSI National Radio Science Meeting*, pp. 1309–1310, 2017.

[16] G. Yang, J. Li, R. Xu, Y. Ma, and Y. Qi, "Improving the performance of wide-angle scanning array antenna with a high-impedance periodic structure," *IEEE Antennas and Wireless Propagation Letters*, vol. 15, pp. 1819–1822, 2016.

[17] P. Karmann, E. Martinod, J. Andrieu, M. Majed, and M. Rammal, "Design of high gain and high steering angle matrix antenna for electronic warfare application," *2022 16th European Conference on Antennas and Propagation (EuCAP)*, pp. 1–5, 2022.

[18] M. Rammal, M. Majed, E. Arnaud, J. Andrieu, and B. Jecko, "Small-size wide-band low-profile "pixel antenna": Comparison of theoretical and experimental results in l band," *International Journal of Antennas and Propagation*, vol. 2019, 2019.

[19] A. Feresidis, G. Goussetis, S. Wang, and J. Vardaxoglou, "Artificial magnetic conductor surfaces and their application to low-profile high- gain planar antennas," *IEEE Transactions on Antennas and Propagation*, vol. 53, no. 1, pp. 209–215, 2005.

[20] H. Abou Taam, M. Salah Toubet, T. Monediere, B. Jecko, and M. Rammal, "A new agile radiating system called electromagnetic band gap matrix antenna," *International Journal of Antennas and Propagation*, vol. 2014, 2014.

[21] B. Jecko, M. Majed, J. Andrieu, M. Lalande, E. Martinod, M. Rammal, and M. T. Themalil, "Overcoming limitations of agile electronically scanned array (aesa) using a radiating surface antenna called agile radiating matrix antenna (arma)," *2021 XXXIVth General Assembly and Scientific Symposium of the International Union of Radio Science (URSI GASS)*, pp. 1–4, 2021.

[22] M. Themalil, M. Majed, M. Rammal, E. Martinod, and B. Jecko, "Miniaturized pixel antenna for implantation on the argos cubesat 4u," *2019 IEEE-APS Topical Conference on Antennas and Propagation in Wireless Communications (APWC)*, pp. 154–156, 2019.

[23] H. Abou Taam, M. Salah Toubet, T. Monediere, B. Jecko, and M. Ram- mal, "Interests of a 1d ebg matrix compared to a patch array in terms of mutual coupling and grating lobe," *2013 7th European Conference on Antennas and Propagation (EuCAP)*, pp. 1045–1048, 2013.

[24] P. Karmann, E. Martinod, J. Andrieu, M. Majed, and M. Rammal, "Design of a high gain, high steering angle and wide band antenna for s band application," *2021 51st European Microwave Conference (EuMC)*, pp. 660–663, 2022.

[25] Xlim, "Presentation of the platinom platform," *Available at https://www.unilim.fr/platinom/* (2022/08/29).

[26] Y. Wen, B. Wang, and X. Ding, "Wide-beam siw-slot antenna for wide-angle scanning phased array," *IEEE Antennas and Wireless Propagation Letters*, vol. 15, pp. 1638–1641, 2016.

[27] Y. Cheng, X. Ding, W. Shao, and C. Liao, "A high-gain sparse phased array with wide-angle scanning performance and low sidelobe levels," *IEEE Access*, vol. 7, pp. 31151–31158, 2019.

[28] G. Yang, Q. Chen, J. Li, S. Zhou, and Z. Xing, "Improving wide-angle scanning performance of phased array antenna by dielectric sheet," *IEEE Access*, vol. 7, pp. 71 897–71 906, 2019.

[29] M. Kamran Ishfaq et al., "Compact Wide-Angle Scanning Multibeam Antenna Array for V2X Communications," *IEEE Antennas and Wireless Propagation Letters*, vol. 20, no. 11, pp. 2141-2145, 2021. DOI: 10.1109/LAWP.2021.3100349.

[30] P. Karmann, E. Martinod, J. Andrieu, and M. Rammal, "Design and simulation of wideband, high gain matrix antenna with beam steering and low side-lobe levels features," *International Journal of Electrical and Computer Engineering Research*, vol. 2, no. 2, p. 22–29, 2022.